doi:10.1017/S1431927615007576 Paper No. 0678 Microsc. Microanal. 21 (Suppl 3), 2015

Microstructure and Strain Hardening in Tensile-Tested Fe-Mn-Al-Si Steels

D. T. Pierce,[1,2] J. A. Jiménez,[3] J. Bentley,[4] D. Raabe,[5] and J. E. Wittig,[1]

[1]Interdisciplinary Materials Science, Vanderbilt University, PMB 351683, Nashville, TN 37232, USA
[2]Now at: Adv. Steel Processing & Products Res. Ctr., Colorado School of Mines, Golden, CO 80401, USA
[3]Centro Nacional de Investigaciones Metalúrgicas (CSIC), Avda Gregorio del Amo 8, 28040-Madrid, Spain
[4]Microscopy and Microanalytical Sciences, PO Box 7103, Oak Ridge, TN 37831-7103, USA
[5]Max-Planck-Institut für Eisenforschung, Max-Planck-Straβe 1, D-40237 Düsseldorf, Germany

The exceptional combination of strength, ductility and strain hardening of high-Mn transformation- and twinning-induced plasticity (TRIP/TWIP) steels makes them appealing for automotive applications (e.g. vehicle weight reductions through down-gauging and room-temperature (RT) forming of complex shaped parts). The present study uses three Fe-22/25/28Mn-3Al-3Si alloys to investigate the effect of changes in stacking-fault energy (SFE) on the evolution of microstructure and mechanical properties during RT tensile deformation. The SFEs were previously measured by analysis of partial-dislocation separations using weak-beam dark-field TEM [1-4] that ultimately [1] incorporated single-crystal elastic constants measured on polycrystalline specimens by a novel nano-indentation method [5,6]. The RT SFEs of the Fe-22/25/28Mn-3Al-3Si alloys are 15±3, 21±3, and 39±5 mJm^{-2}, respectively. Details of alloy and specimen preparation, tensile testing (see Figure 1), and specimen preparation for transmission electron microscopy (TEM) have been described elsewhere [1-4]. Microstructural characterization included optical microscopy, X-ray diffraction and TEM (performed at 200 kV with a Philips CM20T).

The following important conclusions were drawn from this work: (i) A SFE of 15 mJm^{-2} (Fe-22Mn-3Al-3Si) resulted in a deformation microstructure dominated by highly planar slip, suppression of dislocation cross-slip, and $\alpha_{bcc}/\varepsilon_{hcp}$-martensite transformation as the dominant secondary deformation mechanism (see Figure 2). The onset of grain refinement due to the formation of multiple variants of ε_{hcp}-martensite within any given grain occurs from the beginning of plastic deformation and provides superior work hardening at low and intermediate strains (0-0.34 true strain), and the highest strength (687±7 MPa) but lowest elongation (85±3%) of the three alloys. (ii) A SFE of 21 mJm^{-2} (Fe-25Mn-3Al-3Si) resulted in a dislocation structure that exhibits both planar and wavy characteristics. The formation of both ε_{hcp}-martensite and mechanical twinning (see Figure 3) results in excellent strain hardening in the initial, intermediate and final stages of deformation, along with the largest elongation (91±1%) of the three alloys, albeit with intermediate strength (642±7 MPa). (iii) At low strains (0 to 0.1 true strain), a SFE of 39 mJm^{-2} (Fe-28Mn-3Al-3Si) facilitates greater dislocation cross slip and mobility resulting in the formation of a dislocation cell structure (see Figure 4a) and reduced strain hardening compared to that of lower SFE alloys. Formation of ε_{hcp}-martensite is completely suppressed, but mechanical twinning (see Figure 4b) enhances the strain hardening from ~0.1 true strain to failure, resulting in excellent ductility (87±2%) but the lowest strength (631±5 MPa) of the three alloys. (iv) The range of SFE from 15 to 39 mJm^{-2} results in an excellent product of strength and elongation (55-58 GPa%) with only small variations in strength and ductility, despite the transitioning of the steels from TRIP- to TWIP-dominated behavior. Comparisons with literature data indicate that strength and ductility decrease significantly above a SFE of ~40 mJm^{-2}, corresponding to a reduction in mechanical twinning [7].

References:

1. D T Pierce, J A Jiménez, J Bentley, D Raabe, C Oskay, and J E Wittig, *Acta Mater* **68**(2014)238-53
2. D T Pierce, J Bentley, J A Jiménez and J E Wittig, *Scripta Mater* **66**(2012)753-6
3. D T Pierce, J Bentley, J A Jiménez and J E Wittig, Microsc Microanal **17**-Suppl 2(2011)1888-9
4. D T Pierce, J Bentley, J A Jiménez and J E Wittig, Microsc Microanal **18**-Suppl 2(2012)1894-5
5. D T Pierce, K Nowag, A Montagne, J A Jiménez, J E Wittig and R Ghisleni, *Mater Sci Eng* **A578**(2013)134-9
6. D T Pierce, K Nowag, A Montagne, J A Jiménez, J E Wittig and R Ghisleni, Microsc Microanal **19**-Suppl 2(2013)1052-3
7. This work was sponsored by the US National Science Foundation Division of Materials Research, under grant DMR0805295 and by the Ministry of Science and Innovation of Spain, under Grant MAT2012-39124. DTP acknowledges support for extended visits to CENIM, Madrid and MPI, Düsseldorf. JB acknowledges his appointment as *Adjoint* Professor of Materials Science at Vanderbilt University.

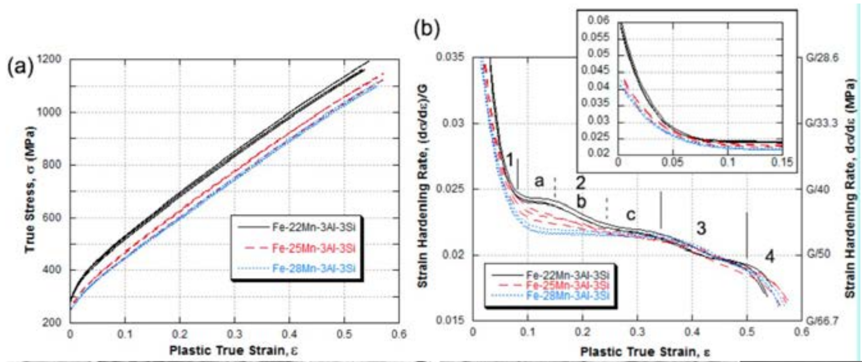

Figure 1. RT tensile data (3 tests for each alloy) at 4 x 10^{-4} s^{-1} using sub-sized flat specimens with 20-mm gauge length, 5-mm width and 1.5-mm thickness. (a) True stress vs true strain. (b) Strain-hardening rate, normalized by the experimental shear modulus (G = 69 GPa), vs true strain. Data in (b) are derivatives of 9^{th} order polynomial fits of data in (a). 4 stages (plus 3 sub-stages for the 22%Mn alloy) of strain hardening are labeled.

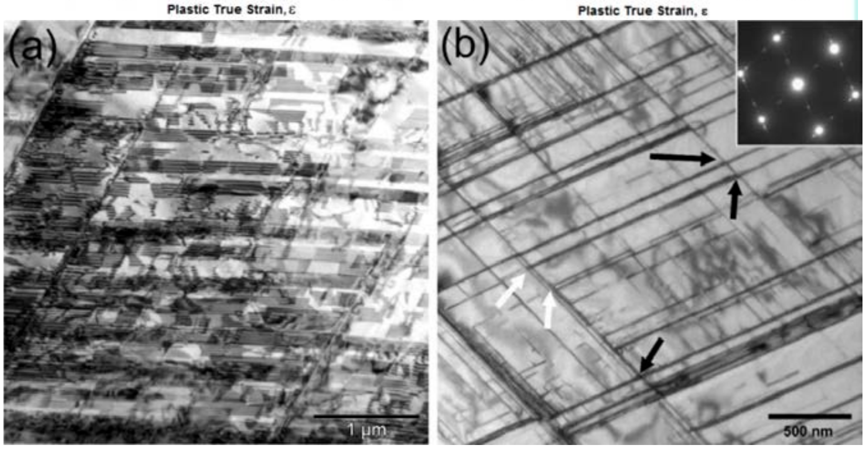

Figure 2. TEM BF images of 22%Mn alloy after 0.1 plastic true strain. (a) High density of overlapping SFs (inclined ε_{hcp}-martensite laths) and (b) grain with 2 variants of edge-on ε_{hcp}-martensite laths oriented with $(111)_\gamma||(0001)_\varepsilon/[1\text{-}10]_\gamma||[1\text{-}210]_\varepsilon$ where γ indicates the austenite matrix. SAD pattern (inset) was recorded at a <110> zone whereas the BF image was recorded slightly off the zone axis in a two-beam condition. Arrows indicate lath intersections (black) or terminations (white).

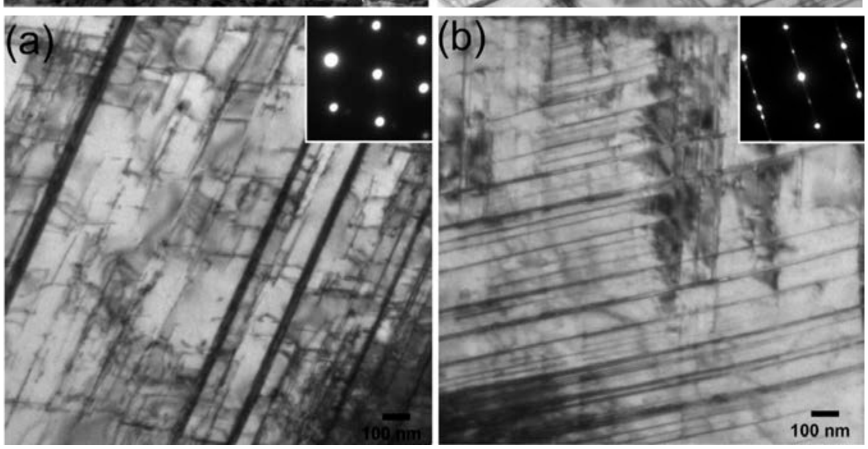

Figure 3. 25%Mn alloy deformed to 0.1 true strain. BF images of (a) mechanical twinning and (b) fine ε_{hcp}-martensite lath structure. The SAD patterns (inset) were recorded at <110> zones whereas the BF images were recorded a few degrees off axis in two beam conditions. SAD patterns show twin reflections at 1/3 positions along <111> rows except through the central spot or ε_{hcp}-martensite reflections also along <111> rows but based on a rectangular net with $(0001)_\varepsilon$ at ~1/2<111> position.

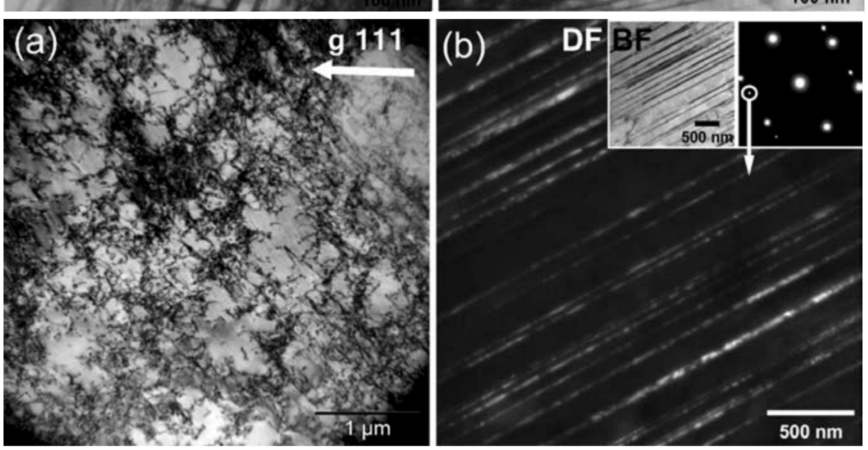

Figure 4. 28%Mn alloy deformed to 0.1 true strain. (a) BF image of grain with dislocation cell structure. (b) DF image of mechanical twins using a {111} twin refection. The SAD pattern and BF image (insets) were recorded at a <011> zone and slightly off axis in a two-beam condition, respectively. 25 and 100% of grains contain mechanical twins for true strains of 0.10 and 0.18, respectively. High densities of dislocations are present in inter-twin regions, especially near twin/matrix interfaces.

https://doi.org/10.1017/S1431927615007576 Published online by Cambridge University Press